J. Appl. Comput. Mech., 11(3) (2025) 681-691
DOI: 10.22055/jacm.2024.47739.4778

ISSN: 2383-4536
jacm.scu.ac.ir

Shahid Chamran University of Ahvaz

Journal of Applied and Computational Mechanics

Research Paper

Parametric Study of Entropy Generation in Magnetohydrodynamic Casson Fluid Flow on a Porous Stretching Sheet under an Inclined Magnetic Field

Sina Sadighi[1], Goodarz Ahmadi[2], Hossein Afshar[3], Hossein Ahmadi Danesh Ashtiani[1], Mohsen Jabbari[1]

[1] Department of Mechanical Engineering, South Tehran Branch, Islamic Azad University, Tehran, Iran,
Email: sinasadighi92@yahoo.com (S.S.); hdanesh1381@yahoo.com (H.A.D.A.); mohsen.jabbari@gmail.com (M.J.)

[2] Department of Mechanical and Aeronautical Engineering, Clarkson University, Potsdam, USA, Email: gahmadi@clarkson.edu

[3] Department of Mechanical Engineering, East Tehran Branch, Islamic Azad University, Tehran, Iran, Email: ho_afshar@yahoo.com

Received August 12 2024; Revised September 21 2024; Accepted for publication September 30 2024.
Corresponding author: H. Afshar (ho_afshar@yahoo.com)

Abstract. This study presents the analytical solutions of the entropy production of magnetohydrodynamic Casson fluid flow on a porous extending sheet. An investigation was conducted to analyze the role of permeability, inclined magnetic force, radiation, Joule dissipation, viscous dissipation, and heat generation/absorption on the momentum and energy equations leading to entropy generation. A closed-form energy equation solution was achieved by utilizing the confluent hypergeometric function. The presented results showed that entropy production is directly related to the Eckert number and inversely related to the Darcy number and the Casson parameter. By increasing the Casson parameter from 0.2 to 100 in the high suction mode, the local Nusselt number was increased by 204.6%.

Keywords: Analytical solutions, MHD, Casson fluid flow, Stretching sheet, Joule heating, Entropy generation.

1. Introduction

A Casson fluid refers to a non-Newtonian fluid that exhibits both shear thinning and yields stress behavior, yet, at higher shear values, it behaves more like a Newtonian fluid. The behavior of a Casson fluid on a stretching surface can be influenced by factors such as shear thinning, yield stress, applied forces, and boundary conditions. Abolbashari et al. [1] studied the entropy production of the Casson nanofluid flow on a stretched sheet using a semi-analytical approach. The authors reported that the decreasing Casson and velocity slip parameters lead to an increase in entropy production. The effects of Joule heating and radiation were studied numerically on a vertical extending sheet by Pal et al. [2]. Their results indicated a direct relationship between the local skin friction coefficient and the Brownian motion parameter. Qing et al. [3] noted that the Hartmann number and porosity parameter boosted entropy generation while decreasing velocity. A porous extending sheet was investigated numerically by Bhatti et al. [4] to determine the entropy production by the MHD flow of Eyring-Powell nanofluid. They observed that magnetic field and fluid parameters were inversely related to velocity. Sadighi et al. [5] found that the porosity of the medium has a direct and inverse relation to the amount of the local skin friction coefficient and heat transfer rate. Medical applications of the presence of magnetic fields include tissue engineering, developing biosensors, and targeted delivery of drugs. As part of their study, El-Aziz et al. [6] numerically studied entropy production over an impermeable sheet for MHD Casson fluid flow with the Hall effect. In their study, it was shown that increasing the Casson parameter decreases entropy generation and Bejan number. A stretching/shrinking surface was used in the study by Gorder et al. [7] to investigate the magnetic parameter on viscous fluid flow. Stretching/shrinking porous sheets occurs in many industries. Some applications are energy absorption, smart textiles, soft robotics, filtration, and separation. Butt et al. [8] utilized convective mass and heat boundary conditions for the porous extended sheets. Their results showed a direct relationship between the averaged entropy production number with solutal and thermal Biot numbers. An investigation was conducted by Shah et al. [9] into the influence of activation energy and chemical reaction parameters on entropy production. After utilizing a semi-analytical method, they concluded that thermal radiation and viscous dissipation effects were directly related to the heat transfer rate. Engineers can design more efficient processes by identifying the sources and magnitudes of entropy production. For example, modifying the material properties of a stretching/shrinking surface could minimize energy dissipation and improve overall performance. For comparisons of different designs or operating conditions, entropy production can be used as a performance metric. Sadighi et al. [10] analytically probed the entropy generation of MHD mixed convection of micropolar fluid

Published online: October 25 2024

flow on an oblique extending surface. They combined three distinct parameters to define a new magneto-buoyancy-inclination parameter. Ramudu et al. [11] studied the convective heat transfer of MHD Casson fluid flow on a vertically extending surface. They stated that the local skin friction is directly related to the Grashof number and velocity slip parameter. Using a semi-analytical method, Sohail et al. [12] calculated the flow field chaos on a nonlinear bi-directional extended sheet. Pal et al. [13] demonstrated that the Brownian motion number and suction parameter directly relate to the local Sherwood number. The Runge-Kutta-Gill procedure was employed by Gangadhar et al. [14] to solve the MHD Casson fluid flow under the Newtonian heating boundary condition. According to the authors, the thickness of the thermal boundary layer is significantly affected by the suction parameter. Sadighi et al. [15] studied MHD heat and mass transfer nanofluid flow on a porous cylinder with chemical reactions. They concluded that the chemical reaction parameter and inverse Darcy number are inversely and directly related to the local Sherwood number. A study by Kumar et al. [16] found that activation energy is inversely related to mass transfer rate. Khan et al. [17] found that stretching or shrinking the impermeable sheet affects the local Nusselt number and skin friction coefficient. Some stagnation point flow applications can be found in the food industry, pharmaceutical manufacturing, and polymer processing. Anusha et al. [18] scrutinized Casson hybrid nanofluid unsteady 2-D stagnation point flow on a porous extending surface. The authors used an incomplete Gamma function to solve the energy equation. Their study proved that mass suction affects skin friction coefficient and heat transfer rate differently. Zhou et al. [19] examined an extending stretching surface to study the unsteady slip flow of magnetohydrodynamic Casson fluid. The study demonstrated that suction and radiation parameters directly affect the local Nusselt number. To solve the energy equation, Mahabaleshwar et al. [20] used an incomplete gamma function to obtain the exact solution. These researchers demonstrated a direct relationship between temperature and suction parameters. A numerical study was conducted by Abbas et al. [21] in order to investigate the MHD Casson hybrid nanofluid flow on an impermeable normal extending surface. Based on the authors' observations, there is an inverse relationship between thermal slip and both heat transfer rate and local skin friction. The unique properties of carbon nanotubes (CNTs) in industrial applications include high strength, thermal conductivity, and electrical conductivity, and their ability to be functionalized with various molecules and biocompatibility make them ideal for medical applications. Sneha et al. [22] analytically performed an entropy analysis for MHD carbon nanotubes flowing over a stretching sheet. They declared that the temperature ratio parameter and Brinkman number directly relate to entropy production. Finally, MHD mixed convection of Casson nanofluid flow was investigated numerically by Ali et al. [23] in order to clarify the effect of Arrhenius activation energy. Their study concluded that entropy generation is a function of dimensionless numbers, including Brinkman, thermal Biot, and solute Biot, as well as parameters like radiation, thermophoresis, and Brownian motion. An investigation by Abdal et al. [24] examined the role of physical phenomena on the behavior of Williamson and Maxwell nanofluid over a stretching permeable surface subjected to a Cattaneo-Christov diffusion. As noted in their study, the Sherwood number is directly related to the Schmidt number, dimensionless reaction rate, temperature difference, and power law index. An investigation conducted by Bejawada et al. [25] showed that the Prandtl number and the radiation parameter have an inverse relationship with local skin friction. Finally, a study by Biswas et al. [26] sought to evaluate the influences of the Hall current and chemical reaction over a Casson nanofluid flow over a normal sheet. Their study illustrated that local skin friction is inversely related to the chemical reaction parameter and Soret number. Recently, Sharma and Shaw [27] studied the effect of radiation and viscous dissipation on the MHD flow of a non-Newtonian fluid past a stretching sheet. Mahabaleshwar et al. [28] investigated the radiation effect on the stagnation point flow of Casson nanofluid past a stretching plate/cylinder. Flows of Casson nanofluid over stretching with heat transfer were studied by Hafez et al. [29]. Saha et al. [30], Mallick et al. [31], and Biswas et al. [32] described the effect of obstructing blocks on enhanced heat transfer in various flows. Additional studies of Casson and other nanofluid flow in different applications were reported in [33-42]. These studies have enhanced our understanding of nanofluid behavior and paved the way for better design and optimizing fluid flow for different applications.

The presented literature survey shows that a systematic parametric study of the entropy generation of the MHD Casson fluid on an extending surface was not reported earlier. The current study focuses on examining the flow and temperature field of MHD Casson fluid over a permeable extending surface in the laminar flow regime. The investigation takes into account the impact of various factors, such as a magnetic field, the permeability of the medium, thermal radiation, viscous dissipation, Ohmic heating, and heat generation/absorption. The governing PDEs and boundary conditions for laminar boundary layer flows were reduced to a set of ODEs using the similarity transformation. An exact solution for the nonlinear momentum equation was first obtained. Then, using an intermediate variable, the exact solution of the energy equation was derived using the hypergeometric Kummer's function. Finally, a parametric study of the role of the different parameters on the velocity and temperature distributions, the local skin friction coefficient, heat transfer rate, entropy generation, and Bejan parameters was performed. It was found that suction/injection and radiation parameters significantly affect the heat transfer of Casson fluids. One main novelty of this study is the mathematical procedure for obtaining analytical solutions for evaluating the entropy and Bejan parameters. In addition, the potential applications to biological and industrial flows and heat transfer are discussed.

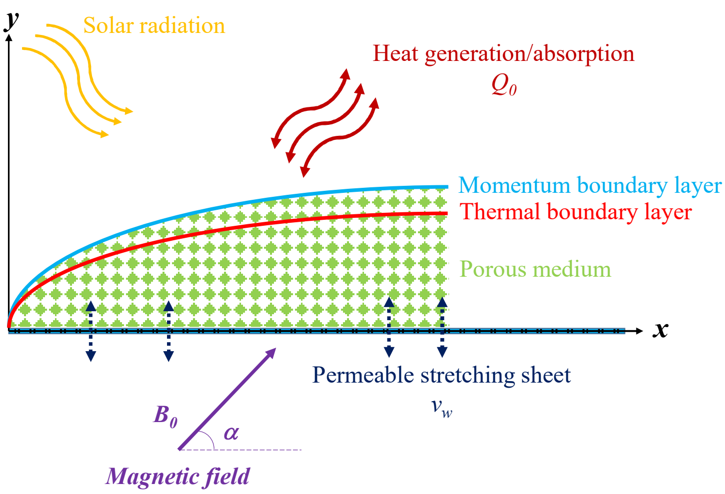

Fig. 1. Physical model and coordinate system.

2. Problem Formulation

We assume an incompressible, steady, 2-D, laminar Casson fluid flow field on a permeable extending sheet. The inclined magnetic field is directed to the surface, as shown in Fig. 1. The submerged, porous stretching surface is stretched in the x-direction through an electrically conducting fluid. The temperature and velocity of the wall are $T_w(x) = T_\infty + bx^2$ and $u_w(x) = ax$, respectively.

The equation that describes the flow behavior of an incompressible and isotropic Casson fluid is known as the rheological equation and can be expressed as follows [43]:

$$\tau_{ij} = \begin{cases} 2\left(\mu_B + \dfrac{P_y}{\sqrt{2\pi}}\right)d_{ij}, \ \pi > \pi_c \\ 2\left(\mu_B + \dfrac{P_y}{\sqrt{2\pi_c}}\right)d_{ij}, \ \pi < \pi_c \end{cases} \tag{1}$$

where P_y is the Casson fluid yield stress, τ_{ij} is the stress tensor, d_{ij} is the deformation rate, μ_B is plastic dynamic viscosity, $\pi = d_{ij}d_{ji}$ is the product of the component of deformation rate with itself, and π_c is the critical value of π. The governing boundary layer equations for the MHD Casson fluid flow and energy conservation are as follows [44]:

$$\frac{\partial u}{\partial x} + \frac{\partial v}{\partial y} = 0 \tag{2}$$

$$u\frac{\partial u}{\partial x} + v\frac{\partial v}{\partial y} = \nu\left(1+\frac{1}{\beta}\right)\left(\frac{\partial^2 u}{\partial y^2}\right) - \frac{\sigma_f B_0^2}{\rho_f}\sin^2(\alpha)u - \frac{\mu_f}{\rho_f K_0}u \tag{3}$$

Here, $\nu = \mu_B / \rho$ is kinematic viscosity, and $\beta = \mu_B\sqrt{2\pi_c} / P_y$ is the Casson parameter.

$$(\rho c_p)_f\left(u\frac{\partial T}{\partial x} + v\frac{\partial T}{\partial y}\right) = k_f\left(\frac{\partial^2 T}{\partial y^2}\right) - \frac{\partial}{\partial y}(q_r) + \mu_B\left(1+\frac{1}{\beta}\right)\left(\frac{\partial u}{\partial y}\right)^2 + \sigma_f B_0^2\sin^2(\alpha)u^2 + \frac{\mu_f}{K_0}u^2 + Q_0(T-T_\infty) \tag{4}$$

The Roseland approximation is used to account for the thermal radiation as:

$$q_r = -\frac{4\sigma^*}{3k^*}\frac{\partial T^4}{\partial y} \tag{5}$$

Accordingly, T^4 is expanded as a Taylor series about "T_∞" and approximated after neglecting higher-order terms. That is, $T^4 \approx T_\infty^4 + 4T_\infty^3 T_1$, where $T_1 = T - T_\infty$. The updated PDE can be written as follows once the energy equation is substituted:

$$(\rho c_p)_f\left(u\frac{\partial T}{\partial x} + v\frac{\partial T}{\partial y}\right) = k_f\left(\frac{\partial^2 T}{\partial y^2}\right) - \frac{16\sigma^* T_\infty^3}{3k^*}\frac{\partial^2 T}{\partial y^2} + \mu_B\left(1+\frac{1}{\beta}\right)\left(\frac{\partial u}{\partial y}\right)^2 + \sigma_f B_0^2\sin^2(\alpha)u^2 + \frac{\mu_f}{K_0}u^2 + Q_0(T-T_\infty) \tag{6}$$

The boundary conditions are:

$$y = 0\begin{cases} u = u_w(x) = ax, v = v_w \\ T = T_w(x) = T_\infty + bx^2 \end{cases}$$

$$u \to 0, \ T \to T_\infty, \ as \ y \to \infty,$$

The relevant similarity variables to solve PDEs are:

$$\eta = y\sqrt{\frac{a}{\nu_f}}, \ u = axf'(\eta), \ v = -\sqrt{a\nu_f}\,f(\eta), \ \theta(\eta) = \frac{T-T_\infty}{T_w - T_\infty} \tag{7}$$

2.1. Similarity solution

In certain classes of problems, the dependent variables are functions of a combination of the independent variables. In these cases, using the similarity transformation reduces the governing partial differential equations to the ordinary differential equations that simplify the solution procedure. The similarity variables depend on the physics and geometry of the problem, as well as the boundary conditions. Here, the similarity variables defined in Eq. (7) are used. In addition to the evaluation of the velocity and temperature fields, the similarity solutions also allow the evaluation of the local skin friction coefficient and Nusselt number.

Inserting the expression given by Eq. (7) into Eqs. (3) and (4) the resulting highly nonlinear coupled ODEs are:

$$\left(1+\frac{1}{\beta}\right)f''' + ff'' - f'^2 - \left(Ha\sin^2(\alpha) + Da\right)f' = 0 \tag{8}$$

$$(1+Rd)\theta'' + \Pr\left[(f\theta' - 2f'\theta) + Ec\left(\left(1+\frac{1}{\beta}\right)f''^2 + \left(Ha\sin^2(\alpha) + Da\right)f'^2\right) + Q\theta\right] = 0 \tag{9}$$

After using Eq. (7) in Eqs. (5) and (6), the new boundary conditions for the similarity variables are given as:

$$f(0) = s, \ f'(0) = 1, \ \theta(0) = 1 \tag{10}$$

$$f'(\infty) \to 0,\ \theta(\infty) \to 0 \tag{11}$$

The local skin friction coefficient and Nusselt number of the Casson fluid flow under the influence of the physical parameters are:

$$C_f = \frac{\mu_f}{\rho_f u_w^2(x)}\left(\frac{\partial u}{\partial y}\right)_{y=0},\quad Nu_x = \frac{-x\left(k_f + \dfrac{16\sigma^* T_\infty^3}{3\left(\rho c_p\right)_f}\right)}{k_f\left(T_w - T_\infty\right)}\left(\frac{\partial T}{\partial y}\right)_{y=0} \tag{12}$$

By using the similarity variable, the skin friction coefficient and the Nusselt number may be restated as:

$$\mathrm{Re}_x^{1/2} C_f = \left(1+\frac{1}{\beta}\right)f''(0),\ \mathrm{Re}_x^{-1/2} Nu_x = -(1+Rd)\theta'(0) \tag{13}$$

3. Exact Solutions

3.1. Momentum equation

According to the boundary conditions, an exponential solution is assumed [45]. That is:

$$f(\eta) = s + \frac{1-e^{-\lambda\eta}}{\lambda},\quad \lambda > 0 \tag{14}$$

Using Eq. (14) in Eq. (8), the algebraic equation for evaluating λ is given as:

$$\left(1+\frac{1}{\beta}\right)\lambda^2 - \lambda s - \left(Ha\sin^2(\alpha) + Da + 1\right) = 0 \tag{15}$$

The solution of Eq. (15) is:

$$\lambda = \frac{\beta s \pm \sqrt{\beta\left[\beta s^2 + 4(1+\beta)\left(Ha\sin^2(\alpha) + Da + 1\right)\right]}}{2(1+\beta)} \tag{16}$$

However, only the positive value of λ is acceptable to satisfy the boundary conditions.

3.2. Energy equation

For achieving an analytical solution for the temperature field, it is assumed that $\theta(\varsigma)$, where ς is a function of η given as:

$$\varsigma = -\frac{\Pr e^{-\lambda\eta}}{(1+Rd)\lambda^2},\ \frac{\partial\varsigma}{\partial\eta} = -\lambda\varsigma,\ \frac{\partial\theta}{\partial\eta} = -\lambda\varsigma\frac{\partial\theta}{\partial\varsigma},\ \frac{\partial^2\theta}{\partial\eta^2} = \lambda^2\varsigma\left(\varsigma\frac{\partial^2\theta}{\partial\varsigma^2} + \frac{\partial\theta}{\partial\varsigma}\right) \tag{17}$$

After the above transformation, the simplified energy equation is given as:

$$\varsigma\frac{\partial^2\theta}{\partial\varsigma^2} + (1-c-\varsigma)\frac{\partial\theta}{\partial\varsigma} + \left(2+\frac{q}{\varsigma}\right)\theta = -r\varsigma\ , \tag{18}$$

where,

$$c = \frac{\Pr(1+s\lambda)}{(1+Rd)\lambda^2},\ q = \frac{Q\Pr}{(1+Rd)\lambda^2},\ r = \frac{\lambda^2 \mathrm{Ec}(1+Rd)\left[\lambda^2\left(1+\dfrac{1}{\beta}\right) + Ha\sin^2(\alpha) + Da\right]}{\Pr} \tag{19}$$

The transformed boundary conditions are then given as:

$$\theta(0) = 0,\ \theta(1) = 1 \tag{20}$$

Solving the transformed ODE along transformed boundary conditions results in an analytical solution:

$$\theta(\eta) = c_1 e^{-\lambda\eta K} F\left(k-2, (k+1)(k+1-c)+q, -\frac{\Pr e^{-\lambda\eta}}{(1+Rd)\lambda^2}\right) + c_2\left(\frac{\Pr e^{-\lambda\eta}}{(1+Rd)\lambda^2}\right)^2, \tag{21}$$

where

$$c_1 = \frac{1 - c_2\left(\dfrac{\Pr e^{-\lambda\eta}}{(1+Rd)\lambda^2}\right)^2}{F\left(k-2, (k+1)(k+1-c)+q, -\dfrac{\Pr}{(1+Rd)\lambda^2}\right)},\ c_2 = -\frac{\dfrac{\lambda^2 \mathrm{Ec}(1+Rd)\left[\lambda^2\left(1+\dfrac{1}{\beta}\right) + Ha\sin^2(\alpha) + Da\right]}{\Pr}}{4 - 2\left(\dfrac{\Pr(1+s\lambda)}{(1+Rd)\lambda^2}\right) + \dfrac{Q\Pr}{(1+Rd)\lambda^2}} \tag{22}$$

Here $F(\alpha,\beta,x)$ is the confluent hypergeometric Kummer's function. The analytical solutions to the momentum and energy equations are obtained, so the solutions of the skin friction coefficient and local Nusselt numbers are also exact. One of the advantages of these parametric solutions is that other publications could validate their outcomes with these solutions.

3.3. Analytical Solution and Confluent hypergeometric function

In this study a similarity solution was used to reduce the governing partial differential equations to a set of differential equations. The differential equation for the momentum equation was solved analytically using an exponential expression. The lambda parameter was then evaluated as given by Eq. (16). We made a change of variable from η to ς in the similarity form of the energy equation, as indicated by Eq. (17). After some simplifications, the ODE takes the form of Kummer's differential equation, and the solution is given in terms of the generalized confluent hypergeometric function. The solution's constants are obtained using the boundary condition. A specific method is also used to evaluate the particular solution [46-48].

4. Entropy Generation Analysis

The novelty of this paper is to provide a mathematical solution to the entropy generation and Bejan number of MHD Casson fluid flow immersed in a porous medium. The mathematical definition of entropy production is as follows [49]:

$$S'''_{gen}=\underbrace{\frac{k_f}{T_\infty^2}\left[\left(\frac{\partial T}{\partial x}\right)^2+\left(1+\frac{16\sigma^* T_\infty^3}{3k^*}\right)\left(\frac{\partial T}{\partial y}\right)^2\right]}_{S'''_{Th}}+\underbrace{\frac{\mu_f}{T_\infty^2}\left(1+\frac{1}{\beta}\right)\left(\frac{\partial u}{\partial y}\right)^2+\frac{\mu_f}{T_\infty K_0}u^2}_{S'''_{Ff}}+\underbrace{\frac{\sigma_f B_0^2}{T_\infty}\sin^2(\alpha)u^2}_{S'''_{Jd}} \tag{23}$$

Here S'''_{Th}, S'''_{Ff}, S'''_{Jd} and are entropy production due to heat transfer, fluid friction, and Joule dissipation. Dividing Eq. (23) by the characteristic rate of entropy generation, $S'''_0=k_f(\Delta T)^2/L^2T_\infty^2$, and restating the variables in similarity form using Eq. (7), it follows that:

$$E_g(\eta,\chi)=\frac{S'''_{gen}}{S'''_0}=\frac{4}{\chi^2}\theta^2+(1+Rd)\mathrm{Re}\,\theta'^2+\left(1+\frac{1}{\beta}\right)\frac{\Pr Ec\mathrm{Re}}{Td}f''^2+\frac{\Pr Ec\mathrm{Re}\left(Ha\sin^2(\alpha)+Da\right)}{Td}f'^2 \tag{24}$$

where $\chi=x/L$, $\mathrm{Re}=aL^2/\nu_f$ and $Td=\Delta T/T_\infty$, respectively, are the dimensionless distance in the x-direction, Reynolds number, and dimensionless temperature ratio. Another significant thermodynamic quantity is the Bejan parameter, which quantifies how much entropy has been produced due to heat transfer in a system relative to total entropy production. That is:

$$Be(\eta,\chi)=\frac{1}{1+\dfrac{\left(1+\frac{1}{\beta}\right)\frac{\Pr Ec\mathrm{Re}}{Td}f''^2+\frac{\Pr Ec\mathrm{Re}\left(Ha\sin^2(\alpha)+Da\right)}{Td}f'^2}{\frac{4}{\chi^2}\theta^2+(1+Rd)\mathrm{Re}\,\theta'^2}} \tag{25}$$

The Bejan parameter is in the range of $0\le Be(\eta)\le 1$. The value of $Be(\eta)\approx 1$ indicates that entropy production by heat transfer is more than that of viscous dissipation and Joule dissipation.

5. Results and Discussion

The analytical solutions for the laminar MHD Casson fluid flow problem on a porous extending surface are given by Eqs. (14) and (21). These solutions are used to perform a series of parametric studies of the effects of the Hartmann number, Casson parameter, suction/injection parameter, radiation parameter, Prandtl number, source/sink parameter, and Eckert number on the flow and thermal boundary layers, as well as, the variation of the local skin friction coefficient and local Nusselt number.

5.1. Velocity distribution

The effects of the fluid suction/injection, inverse Darcy number, Harman number, and Casson parameter on the velocity boundary layers are studied in this section. The impact of s on the velocity distribution is demonstrated in Fig. 2. Fluid velocity decreases in the suction mode compared to the injection mode when the stretching sheet is permeable. So, injection at the wall increases the velocity magnitude and consequently increases the boundary layer thickness (VBLT). Figure 2 also shows that increasing the inverse Darcy number decreases the velocity boundary layer thickness. The enhanced friction and altered velocity profile in a porous medium can reduce the VBLT. The porous medium tends to slow down the fluid more effectively near the wall, compressing the boundary layer. It was found that by decreasing the suction/injection parameter in Fig. 2 from 4 to -4 for the impermeable medium, the value of $\mathrm{Re}_x^{1/2}C_f$ (given by Eq. (13)) changes from -4.976 to -0.976 and increases by 80.38%. On the other hand, for the permeable medium, the value of $\mathrm{Re}_x^{1/2}C_f$ changes from -4.996 to -0.996 and increases by 80.06%.

The effect of the Casson parameter on the boundary layer velocity profile is shown in Fig. 3. Despite the presence (Ha = 10) or absence (Ha = 0) of inclined magnetic fields, decreasing the Casson parameter increases the VBLT. It should be noted that an increase in the Casson parameter enhances plastic dynamic viscosity and increases fluid flow resistance. The non-Newtonian fluids, therefore, produce more resistance when compared to Newtonian fluids due to their enhanced viscosity. The Lorentz force is generated when an inclined magnetic field is exerted, producing a resistive force. Fig. 3 shows that due to the enhancement of the resistive force, the VBLT is reduced. That is, the Lorentz force opposes the flow, increasing the drag and reducing the VBLT. A further finding shown in Fig. 3 is that without a magnetic field effect, an increase from 0.1 to 2 in the Casson parameter enhances $\mathrm{Re}_x^{1/2}C_f$ (Eq. (13)) from -2.54 to -0.60, and in terms of percentage, it is enhanced by 76.21%. Meanwhile, in the presence of the Lorentz force, it increases from -10.07 to -3.19 or 68.3%.

5.2. Temperature distribution

As shown in Figs. 4 and 5, several parameters affect the temperature distributions. For fixed values of $s=2,\beta=0.8,Ha=1,Da^{-1}=0.01,Q=-10,$ and $Ec=0.3$ the influence of Pr, and Rd, on temperature variation and thermal boundary layer are studied in Fig. 4. It is evident from the figure that the thickness of the thermal boundary layer (TBLT) increases as the

Prandtl number decreases. Physically, the Prandtl number rises when the fluid viscosity increases and the thermal conductivity of the Casson fluid decreases. A comparison is shown in Fig. 4 between the effect of the presence of the radiation parameter (*Rd* = 10) and its absence (*Rd* = 0). The increased radiative heat flux can result in higher temperature gradients, leading to a thicker TBLT. A wall that absorbs solar radiation causes its temperature to rise, leading to an increase in the fluid temperature. As a result, the thickness of the thermal boundary layer increases. A careful evaluation of Fig. 4 indicates that $\mathrm{Re}_x^{-1/2} Nu_x$ is directly related to the Prandtl number. By increasing the Prandtl number from 3 to 9, $\mathrm{Re}_x^{-1/2} Nu_x$ (Eq. (13)), in the absence of thermal radiation, it rises from 8.99 to 20.84, showing a 131.91% increase. On the other hand, for *Rd* = 10, the thermal radiation effect increases $\mathrm{Re}_x^{-1/2} Nu_x$ from 21.77 to 41.76 (shows a 91.85% increase).

For under suction mode, $s = 10, \beta = 2, Ha = 5, Da^{-1} = 0.05, \mathrm{Pr} = 6.2$ and $Rd = 5$, Fig. 5 illustrates the effect of variation of Q, and *Ec*, on the temperature variations and TBLT over a stretching sheet. Heat is produced in thermal boundary layers by $+Q$ and *Ec*. The TBLT enhances as the heat source parameter and Eckert number increase. When *Ec* is high, viscous dissipation is significant, meaning that a considerable amount of the fluid's kinetic energy is converted into heat. Figure 5 shows that a change from the heat absorption $Q = -10$ to the heat generation $Q = 10$ results in a decline in the $\mathrm{Re}_x^{-1/2} Nu_x$. For *Ec* = 0, as the heat generation/absorption parameter rises from -10 to 10, the value of $\mathrm{Re}_x^{-1/2} Nu_x$ (given by Eq. (13)) declines from 68.43 to 56.52, by 17.41%. Meanwhile, with the high Eckert number (*Ec* = 1), it decreases from 35.03 to 18.16 by 48.16%.

The porous medium wall boundaries are present in many practical applications. Flows in biological tissues, heat exchangers, and electronic cooling are some examples of porous medium walls. Figure 6 displays the effect of the magnetic field's inclination parameter ($B_{effective} = B_0 \sin\alpha$) and Darcy number (*Da*) on temperature distribution in the boundary layer. An increase of both α and *Da* increases the TBLTs. It is important to note that both of these parameters significantly impact the local Nusselt number. According to Eq. (13), the local Nusselt number decreases by 105% with the porous medium, whereas it decreases by 115% without the porous medium.

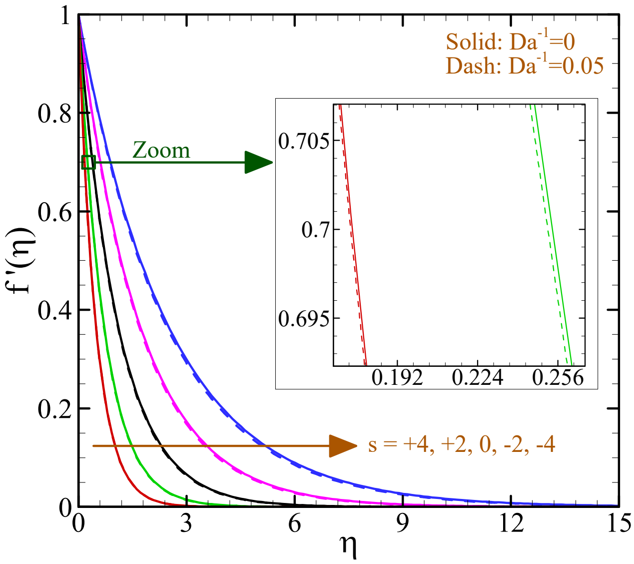

Fig. 2. Effect of suction/injection parameter on the boundary layer velocity profile for $\alpha = \pi/4, \beta = 0.7$, and $Ha = 2$.

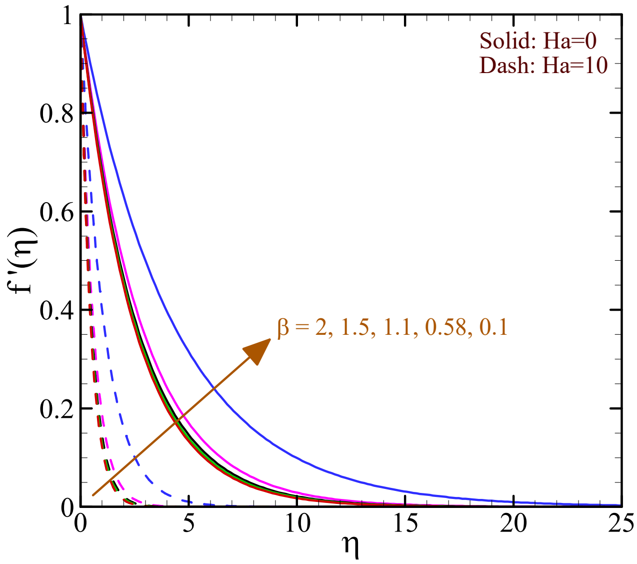

Fig. 3. Effect of Casson parameter on the boundary layer velocity profile for $\alpha = \pi/2, s = -2$, and $Da^{-1} = 0.05$.

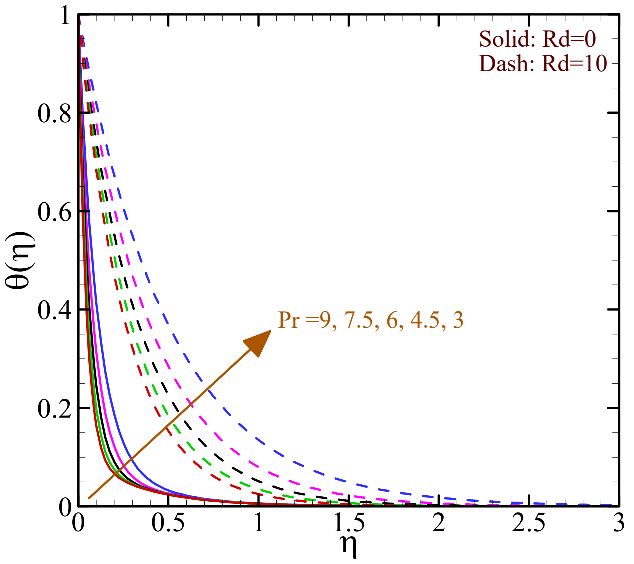

Fig. 4. Effect of Prandtl number on the temperature boundary layer when $\alpha = \pi/2, s = 2, \beta = 0.8, Ha = 1, Da^{-1} = 0.01, Q = -10$, and $Ec = 0.3$.

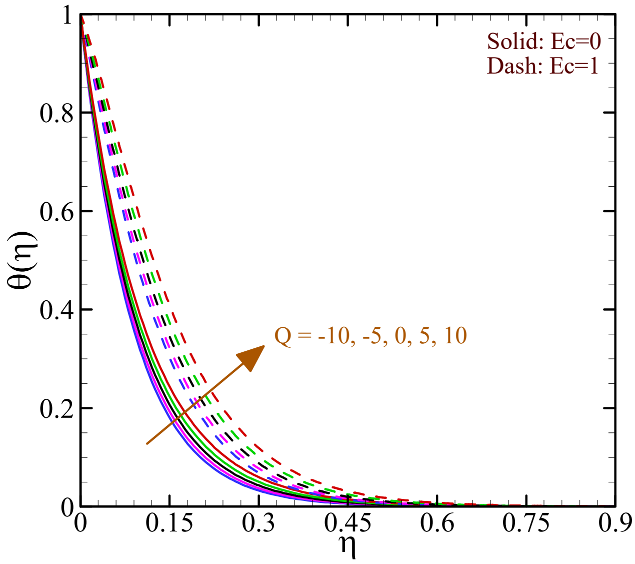

Fig. 5. Effect of heat generation/absorption parameter on the temperature boundary layer when $\alpha = \pi/2, s = 10, \beta = 2, Ha = 5, Da^{-1} = 0.05, \mathrm{Pr} = 6.2$, and $Rd = 5$.

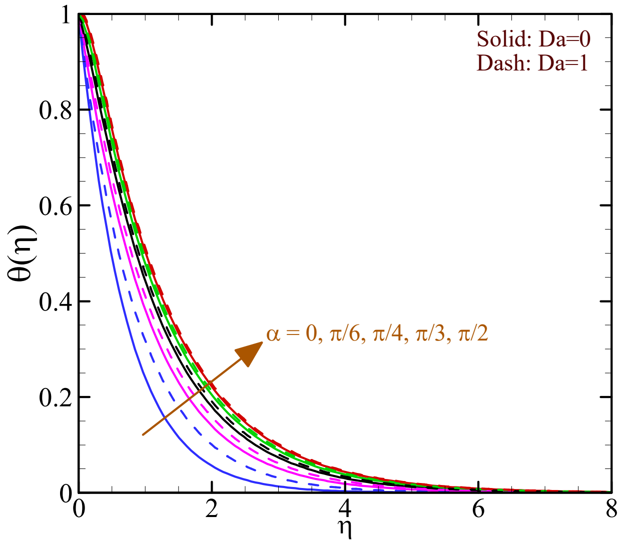

Fig. 6. Effect of magnetic field inclination parameter on the temperature boundary layer when $s=-1, \beta=5, Ha=10, \Pr=4, Rd=2, Q=-1$, and $Ec=0.4$.

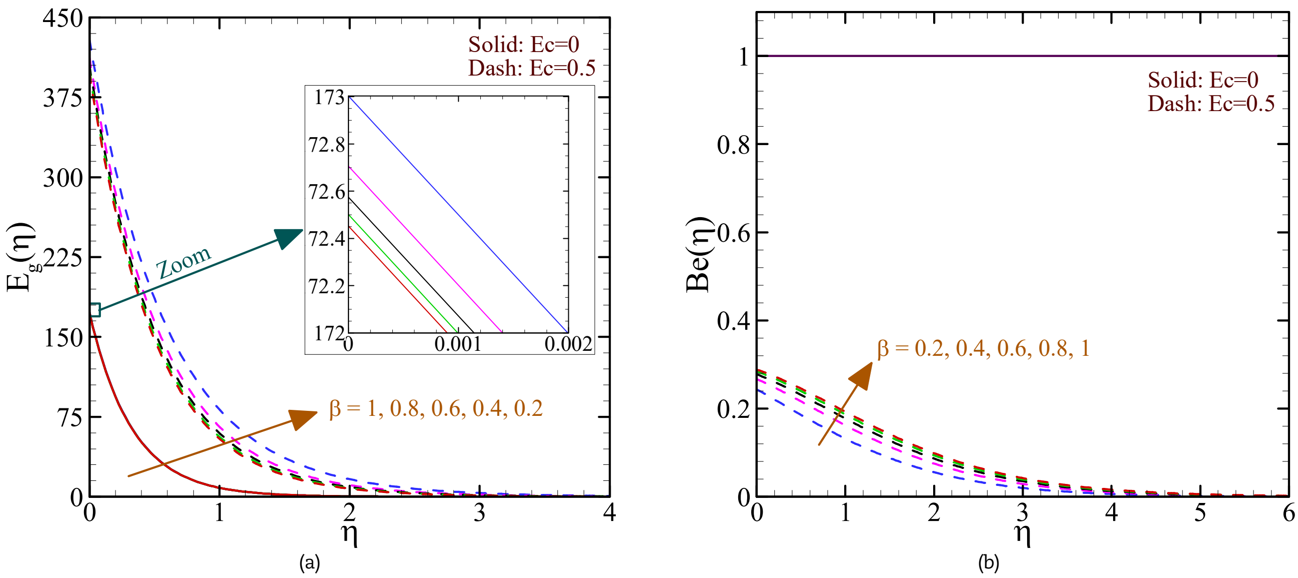

Fig. 7. Effect of Casson parameter on (a) entropy generation and (b) Bejan parameters for $\alpha=\pi/2, s=-10, Ha=10, Da^{-1}=0.05, \Pr=3, Rd=8, Q=-20, \chi=0.7, \text{Re}=8$, and $Td=0.5$ for different values of Ec.

5.3. Analysis of entropy generation

The entropy generation and the Bejan parameter play significant roles in heat transfer and fluid flow. These parameters indicate the system's irreversibility, energy dissipation, and efficiency. Fig. 7 (a and b) illustrates the impact of the Casson parameter and the Eckert number under the high injection (-10) and heat absorption parameters (-20) on the entropy generation and Bejan parameters. In response to the increasing Casson parameter, Fig. 7(a) shows a reduction in the energy of the MHD fluid; hence, the entropy also decreases. Figure 7(b) illustrates that the Bejan parameter is directly related to the Casson parameter under these conditions. This figure also indicates that as the Eckert number decreases to zero, the contribution of heat transfer becomes more and more significant until it reaches the maximum that can be reached. As previously stated, raising the Eckert number generates more internal heat. So, despite the high heat sink effect, this dimensionless number significantly amplified the entropy generation.

Figure 8 (a and b) depicts the effect of Hartmann and inverse Darcy numbers on the entropy production and Bejan parameter for a high injection rate and heat source effect for $s=10, \beta=0.2, \Pr=4, Rd=7, Q=2, Ec=0.1, \chi=0.9, \text{Re}=1$, and $Td=0.1$. Increasing the entropy produced on a porous stretching sheet is achieved by exerting and enhancing the inclined magnetic field (Fig. 8(a)). It is also worth noting that increasing the inverse Darcy number increases entropy production slightly. So, this plot shows that any resistive force that increases the temperature causes entropy production. Considering that the Hartman and inverse Darcy numbers increase, the contribution of fluid friction and Joule dissipation rises, so the Bejan parameter decreases (Fig. 8(b)).

Figure 9 (a and b) illustrates the relation between the Rd and the entropy generation and Bejan parameter subjected to the high Casson parameter and the low Eckert number for $s=-2, \beta=5, Ha=8, Da^{-1}=0.03, \Pr=3, Q=-5, Ec=0.1, \chi=0.2$, and $Td=1.3$. As the intensity of the solar rays intensifies, the temperature of the MHD Casson fluid increases, which causes the entropy to rise when the values of the injection mode, heat absorption effect, and the Eckert number of the fluid are low (Fig. 9(a)). As can be seen from Eq. (24), the entropy generation depends on the Reynolds number. MHD Casson fluid flows faster if the Reynolds number is raised because the inertia forces increase while the viscous forces decrease. Figure 9(b) indicates that reducing the Reynolds number decreases fluid friction and Joule heating contributions, decreasing the Bejan parameter.

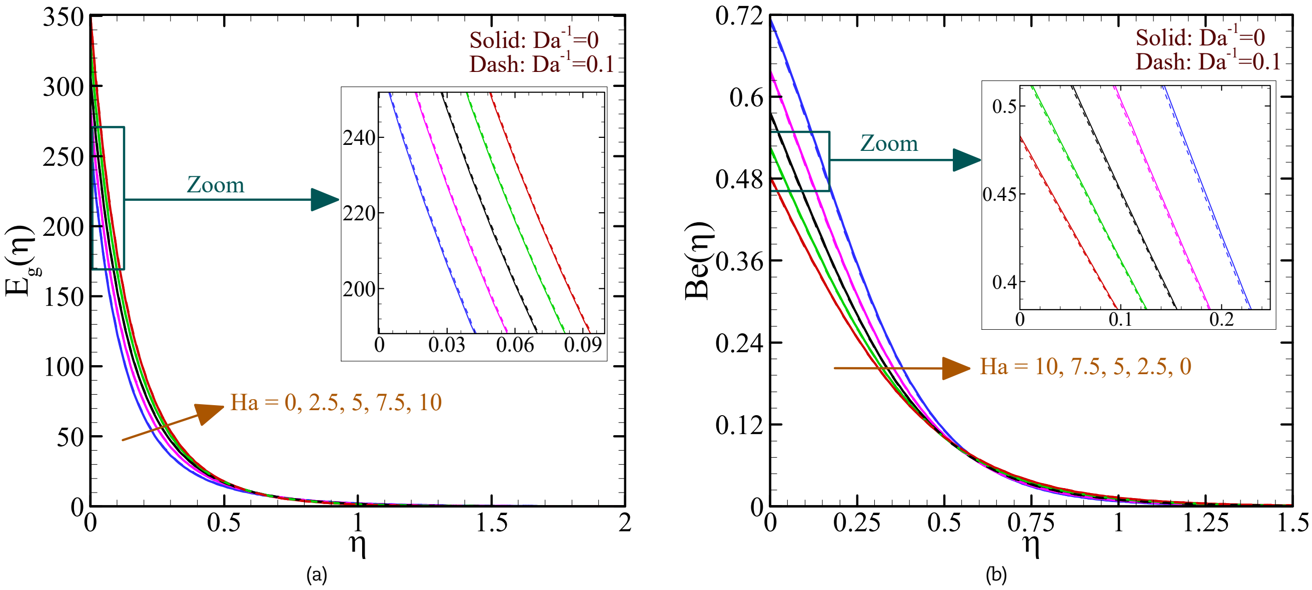

Fig. 8. Effect of Hartmann number on (a) entropy generation and (b) Bejan parameters for $\alpha = \pi / 2, s = 10, \beta = 0.2, \Pr = 4, Rd = 7, Q = 2, Ec = 0.1, \chi = 0.9, \mathrm{Re} = 1$, and $Td = 0.1$ for different values of Da^{-1}.

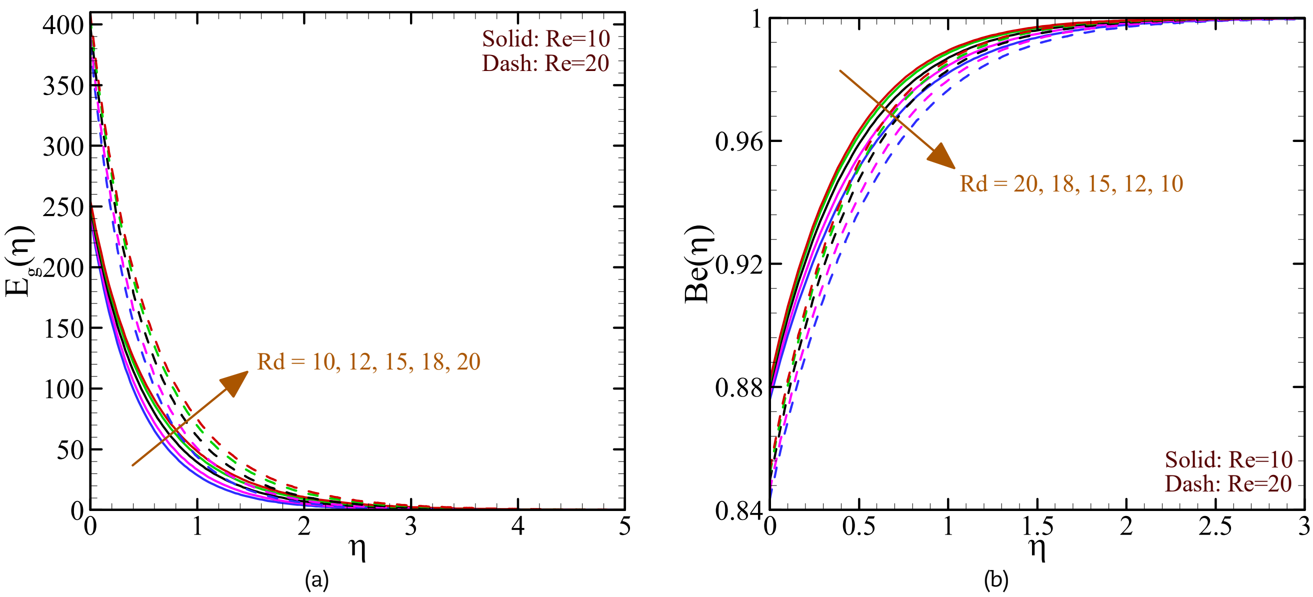

Fig. 9. Effect of radiation parameter on (a) entropy generation and (b) Bejan parameters for $\alpha = \pi / 2, s = -2, \beta = 5, Ha = 8, Da^{-1} = 0.03, \Pr = 3, Q = -5, Ec = 0.1, \chi = 0.2$, and $Td = 1.3$ for different values of Re.

5.4. Model validation and discussion

This section provides a discussion of model validation and accuracy. Table 1 compares the present prediction for the local Nusselt numbers for a range of Prandtl numbers to those of Grubka and Bobba [50] to ensure that the obtained results agree with their previous findings. It is seen that the present model predictions are very close to the earlier study of [50] for the range of parameter values considered.

Table 1. Comparison of heat transfer rate for different Prandtl numbers with previously published results for fluid flow, with $\alpha = \beta = Ha = Da^{-1} = Rd = Ec = Q = s = 0$.

Pr	Grubka and Bobba [50]	Present study
0.01	-0.0294	-0.029416
0.72	-1.0885	-1.088524
1.0	-1.3333	-1.333333
3.0	-2.5097	-2.509725
10.	-4.7969	-4.796873
100.	-15.7120	-15.711967

Table 2. Local Nusselt number values for $\alpha = \pi/2, Ha = 20, Da^{-1} = 0.05, \Pr = 6.2, Rd = 10, Q = -20, Ec = 1$.

β \ s	-4	-2	0	+2	+4
0.2	0.8673	1.7966	3.3274	5.6015	8.6868
1.0	7.5872	9.8861	12.8137	16.3837	20.5448
10.	10.7601	13.8093	17.4033	21.4330	25.7938
100.	11.1730	14.3296	18.0133	22.0932	26.4594

For $\alpha = \pi/2, Ha = 20, Da^{-1} = 0.05, \Pr = 6.2, Rd = 10, Q = -20, Ec = 1$, Table 2 shows the variation of the local Nusselt numbers with the suction/injection s and Casson parameter β. It is seen that the heat transfer is significantly influenced by suction/injection and Casson parameters in the presence of high inclined magnetic field, radiation, heat absorption, and viscous dissipation effects. This table shows that the local Nusselt number is affected by the values of different parameters, as mentioned earlier. So, to have a high local Nusselt number for flows over the porous stretching sheet, it should operate in suction mode (s > 0). Furthermore, Newtonian fluid is superior to non-Newtonian fluid for enhancing heat transfer.

6. Conclusions

This study analytically assessed the entropy production of the MHD Casson fluid flow on a porous extending surface. PST (prescribed surface temperature) boundary condition was used in this case. The similarity solution was used to convert the governing PDEs into ODEs. The exact solution of the energy equation is achieved through utilizing the confluent hypergeometric function. The analyses that were conducted in this study and the presented graphical and tabular results demonstrated the effects of various physical parameters on velocity and temperature distributions, the local skin friction coefficient, the local Nusselt number, the generation of entropy, and Bejan parameters. The main conclusions are:

- The VBLTs are inversely related to s, Da^{-1}, β, and Ha.
- The TBLTs increase by enhancing Rd, Ec, Da, α and Q. In contrast, the TBLT decreases as Pr increases.
- The skin friction coefficient is directly and inversely related to β and s.
- The local Nusselt number increases as s, β and Pr increases, while it decreases when the Q, Da, and α increases.
- The entropy production is boosted by increasing the Ha, Da^{-1}, Rd, Ec, and Re, while it is decreased by increasing β. Increasing Ec from 0 to 0.5 boosted the E_g by 147.8%.
- The Bejan parameter is increased by the increase of β and Rd, and decreases by the rise of Ec, Ha, Da^{-1}, and Re. Increasing Da^{-1} from 0 to 0.1 decreased Be by 0.3264%
- The inclined magnetic field, medium's permeability, and suction mode strongly affect the flow and temperature fields.

Author Contributions

S. Sadighi designed the methodology, analytical solution, and writing—original draft; H. Afshar supervised, reviewed, and edited; H. Ahmadi Danesh Ashtiani supervised, administered, resources, investigator, writing—review, and editing. M. Jabbari was a supervisor, project administrator, and investigator. G. Ahmadi contributed to the mathematical modeling and editing. The manuscript was written through the contributions of all authors. All authors discussed the results and reviewed and approved the final version of the manuscript.

Acknowledgments

The support of Islamic Azad University (South and East Tehran Branches) and Clarkson University is gratefully acknowledged.

Conflict of Interest

The authors declared no potential conflicts of interest concerning the research, authorship, and publication of this article.

Funding

The authors received no financial support for the research, authorship, and publication of this article.

Data Availability Statements

The datasets generated and/or analyzed during the current study are available from the corresponding author upon reasonable request.

Nomenclature

a	A parameter in the expression for characteristic velocity	Td	Dimensionless temperature ratio variable
b	Characteristic temperature	u, v	Fluid velocities
B_0^2	Magnetic field strength	x, y	Surface coordinates
C_p	Specific heat at a constant temperature	***Greek symbols***	
$Da^{-1} = \frac{\mu_f}{aK_0\rho_f}$	Inverse Darcy number (Permeability parameter)	α	Inclination

$Ec = \dfrac{u_w^2}{(C_P)_f (T_w - T_0)}$	Eckert number	ΔT	Temperature difference
$Ha = \dfrac{\sigma_f B_0^2}{a\rho_f}$	Hartmann number	ς	Intermediate variable
K	Power constant	η	Similarity variable
k	Thermal conductivity	θ	Dimensionless temperature
K_0	Permeability of the medium	μ	Dynamic viscosity
k^*	Mean absorption coefficient	μ_B	Plastic dynamic viscosity
$\Pr = \dfrac{(\mu C_P)_f}{k_f}$	Prandtl number	ν	Kinematic viscosity
P_y	Casson fluid yield stress	π_c	Casson fluid yield stress
$Q = \dfrac{Q_0}{a(\rho C_P)_f}$	Heat source/sink parameter	ρ	Density
$q_r = -\dfrac{4\sigma^*}{3k^*}\dfrac{\partial T^4}{\partial y}$	Radiative heat flux	σ	Electrical conductivity
$Rd = \dfrac{16\sigma^* T_\infty^3}{3k_f k^*}$	Radiation parameter	σ^*	Stefan-Boltzmann constant
$\mathrm{Re}_x^{0.5} C_f$	The skin friction coefficient	χ	Dimensionless distance in the x-direction
$\mathrm{Re}_x^{-0.5} Nu_x$	The local Nusselt number	***Subscription***	
$s(>0/<0)$	Suction/injection parameter	f	Fluid
T_∞	Ambient temperature	w	Wall

References

[1] Abolbashari, M.H., Freidoonimehr, N., Nazari, F., Rashidi, M.M., Analytical modeling of entropy generation for Casson nanofluid flow induced by a stretching surface, *Advanced Powder Technology*, 26(2), 2015, 542-552.
[2] Pal, D., Roy, N., Vajravelu, K., Effects of thermal radiation and Ohmic dissipation on MHD Casson nanofluid flow over a vertical nonlinear stretching surface using scaling group transformation, *International Journal of Mechanical Sciences*, 114, 2016, 257-267.
[3] Qing, J., Bhatti, M.M., Abbas, M.A., Rashidi, M.M., Ali, M.E.S., Entropy Generation on MHD Casson Nanofluid Flow over a Porous Stretching/Shrinking Surface, *Entropy*, 18(4), 2016, 123.
[4] Bhatti, M.M., Abbas, T., Rashidi, M.M., Ali, M.E.S., Yang, Z., Entropy Generation on MHD Eyring–Powell Nanofluid through a Permeable Stretching Surface, *Entropy*, 18(6), 2016, 224.
[5] Sadighi, S., Afshar, H., Ashtiani, H.A.D., Jabbari, M., MHD flow and conductive heat transfer on a permeable stretching cylinder: Benchmark solutions, *Case Studies in Thermal Engineering*, 44, 2023, 102886.
[6] Aziz, M.A.E., Afify, A.A., MHD Casson fluid flow over a stretching sheet with entropy generation analysis and Hall influence, *Entropy*, 21(6), 2019, 592.
[7] Gorder, R.A.V., Vajravelu, K., Pop, I., Hydromagnetic stagnation point flow of a viscous fluid over a stretching or shrinking sheet, *Meccanica*, 47, 2012, 31-50.
[8] Butt, A.S., Maqbool, K., Imran, S.M., Ahmad, B., Entropy generation effects in MHD Casson nanofluid past a permeable stretching surface, *International Journal of Exergy*, 31(2), 2020, 150-171.
[9] Shah, Z., Kumam, P., Deebani, W., Radiative MHD Casson Nanofluid Flow with Activation energy and chemical reaction over past nonlinearly stretching surface through Entropy generation, *Scientific Reports*, 10, 2020, 4402.
[10] Sadighi, S., Afshar, H., Jabbari, M., Ashtiani, H.A.D., An analytical approach to entropy production in MHD mixed convection micropolar fluid flow over an inclined porous stretching sheet, *Frontiers in Mechanical Engineering*, 8, 2022, 900316.
[11] Ramudu, A.CV., Kumar, K.A., Sugunamma, V., Sandeep, N., Influence of suction/injection on MHD Casson fluid flow over a vertical stretching surface, *Journal of Thermal Analysis and Calorimetry*, 139, 2020, 3675-3682.
[12] Sohail, M., Shah, Z., Tassaddiq, A., Kumam, P., Roy, P., Entropy generation in MHD Casson fluid flow with variable heat conductance and thermal conductivity over nonlinear bi-directional stretching surface, *Scientific Reports*, 10, 2020, 12530.
[13] Pal, D., Roy, N., Lie Group Transformation on MHD Double-Diffusion Convection of a Casson Nanofluid over a Vertical Stretching/Shrinking Surface with Thermal Radiation and Chemical Reaction, *International Journal of Applied and Computational Mathematics*, 4, 2018, 13.
[14] Gangadhar, K., Kannan, T., Jayalakshmi, P., Sakthivel, G., Dual solutions for MHD Casson fluid over a shrinking sheet with Newtonian heating, *International Journal of Ambient Energy*, 42(3), 2021, 331-339.
[15] Sadighi, S., Jabbari, M., Afshar, H., Ashtiani, H.A.D., MHD heat and mass transfer nanofluid flow on a porous cylinder with chemical reaction and viscous dissipation effects: Benchmark solutions, *Case Studies in Thermal Engineering*, 40, 2022, 102443.
[16] Kumar, A., Tripathi, R., Singh, R., Sheremet, M.A., Entropy generation on double diffusive MHD Casson nanofluid flow with convective heat transfer and activation energy, *Indian Journal of Physics*, 95, 2021, 1423-1436.
[17] Khan, M.R., Elkotb, M.A., Matoog, R.T., Alshehri, N.A., Abdelmohimen, M.A.H., Thermal features and heat transfer enhancement of a Casson fluid across a porous stretching/shrinking sheet: analysis of dual solutions, *Case Studies in Thermal Engineering*, 28, 2021, 101594.
[18] Anusha, T., Huang, H.N., Mahabaleshwar, U.S., Two dimensional unsteady stagnation point flow of Casson hybrid nanofluid over a permeable flat surface and heat transfer analysis with radiation, *Journal of the Taiwan Institute of Chemical Engineers*, 127, 2021, 79-91.
[19] Zhou, J.C., Abidi, A., Shi, Q.H., Khan, M.R., Rehman, A., Issakhov, A., Galal, A.M., Unsteady radiative slip flow of MHD Casson fluid over a permeable stretched surface subject to a non-uniform heat source, *Case Studies in Thermal Engineering*, 26, 2021, 101141.
[20] Mahabaleshwar, U.S., Maranna, T., Sofos, F., Analytical investigation of an incompressible viscous laminar Casson fluid flow past a stretching/shrinking sheet, *Scientific Reports*, 12, 2022, 18404.
[21] Abbas, N., Shatanawi, W., Abodayeh, K., Computational analysis of MHD nonlinear radiation casson hybrid nanofluid flow at vertical stretching sheet, *Symmetry*, 14(7), 2022, 1494.
[22] Sneha, K.N., Mahabaleshwar, U.S., Sharifpur, M., Ahmadi, M.H., Bahrani, M.A., Entropy Analysis in MHD CNTS Flow Due to a Stretching Surface with Thermal Radiation and Heat Source/Sink, *Mathematics*, 10(18), 2022, 3404.
[23] Ali, K., Faridi, A.A., Ahmad, S., Jamshed, W., Hussain, S.M., Eldin, E.S.M.T., Quasi-Linearization Analysis for Entropy Generation in MHD Mixed-

Convection Flow of Casson Nanofluid over Nonlinear Stretching Sheet with Arrhenius Activation Energy, *Symmetry*, 14(9), 2022, 1940.
[24] Abdal, S., Siddique, I., Alrowaili, D., Mdallal, Q.A., Hussain, S., Exploring the magnetohydrodynamic stretched flow of Williamson Maxwell nanofluid through porous matrix over a permeated sheet with bioconvection and activation energy, *Scientific Reports*, 12, 2022, 278.
[25] Bejawada, S.G., Reddy, Y.D., Jamshed, W., Nisar, K.S., Alharbi, A.N., Chouikh, R., Radiation effect on MHD Casson fluid flow over an inclined nonlinear surface with chemical reaction in a Forchheimer porous medium, *Alexandria Engineering Journal*, 61(10), 2022, 8207-8220.
[26] Biswas, R., Ahmmed, S.F., Effects of Hall Current and Chemical Reaction on Magnetohydrodynamics Unsteady Heat and Mass Transfer of Casson Nanofluid Flow Through a Vertical Plate, *Journal of Heat Transfer*, 140(9), 2018, 092402.
[27] Sharma, R.P., Shaw, S., MHD Non-Newtonian Fluid Flow past a Stretching Sheet under the Influence of Nonlinear Radiation and Viscous Dissipation, *Journal of Applied and Computational Mechanics*, 8(3), 2022, 949-961.
[28] Mahabaleshwar, U.S., Maranna, T., Mishra, M., Hatami, M., Radiation effect on stagnation point flow of Casson nanofluid past a stretching plate/cylinder, *Scientific Reports*, 14, 2024, 1387.
[29] Hafez, N.M., Thabet, E.N., Khan, Z., Abd-Alla, A.M., Elhag, S.H., Electroosmosis-modulated Darcy–Forchheimer flow of Casson nanofluid over stretching sheets in the presence of Newtonian heating, *Case Studies in Thermal Engineering*, 53, 2024, 103806.
[30] Saha, A., Chakravarty, A., Ghosh, K., Biswas, N., Manna, N.K., Role of obstructing block on enhanced heat transfer in a concentric annulus, *Waves in Random and Complex Media*, 4, 2022, 1-25.
[31] Mallick, H., Mondal, H., Biswas, N., Manna, N.K., Buoyancy driven flow in a parallelogrammic enclosure with an obstructive block and magnetic field, *Materials Today: Proceedings*, 44(2), 2021, 3164-3171.
[32] Biswas, N., Manna, N.K., Mahapatra, P.S., Enhanced thermal energy transport using adiabatic block inside lid-driven cavity, *International Journal of Heat and Mass Transfer*, 100, 2016, 407-427.
[33] Mandal, D.K., Biswas, N., Manna, N.K., Gayen, D.K., Gorla, R.S.R., Chamkha, A.J., Thermo-fluidic transport process in a novel M-shaped cavity packed with non-Darcian porous medium and hybrid nanofluid: Application of artificial neural network (ANN), *Physics of Fluids*, 34(3), 2022, 033608.
[34] Chatterjee, D., Biswas, N., Manna, N.K., Mandal, D.K., Chamkha, A.J., Magneto-nanofluid flow in cylinder-embedded discretely heated-cooled annular thermal systems: Conjugate heat transfer and thermodynamic irreversibility, *Journal of Magnetism and Magnetic Materials*, 569, 2023, 170442.
[35] Yang, D., Yasir, M. Hamid, A., Thermal transport analysis in stagnation-point flow of Casson nanofluid over a shrinking surface with viscous dissipation, *Waves in Random and Complex Media*, 34(4), 2024, 3177-3191.
[36] Basha, H.T., Sivaraj, R., Stability Analysis of Casson Nanofluid Flow over an Extending/Contracting Wedge and Stagnation Point, *Journal of Applied and Computational Mechanics*, 8(2), 2022, 566-579.
[37] Sadighi, S., Afshar, H., Jabbari, M., Ashtiani, H.A.D., Heat and mass transfer for MHD nanofluid flow on a porous stretching sheet with prescribed boundary conditions, *Case Studies in Thermal Engineering*, 49, 2023, 103345.
[38] Kumar, T.P., Dharmaiah, G., Al-Farhany, K., Abdulkadhim, A., Alomari, M.A., Abdulsada, M.H., Transient conditions effects on electromagnetic Casson fluid flow via stretching surface: System thermal case elaboration, *Numerical Heat Transfer, Part B: Fundamentals*, 84(5), 2023, 539-555.
[39] Bhavana, P.M., Vanitha, G.P., Mahabaleshwar, U.S., Souayeh, B., Effect of magnetohydrodynamic Casson fluid flow on the stretching/shrinking surface, *ZAMM-Journal of Applied Mathematics and Mechanics/Zeitschrift für Angewandte Mathematik und Mechanik*, 103(10), 2023, e202200523.
[40] Fadhel, M.A., Asghar, A., Lund, L.A., Shah, Z., Vrinceanu, N., Tirth, V., Dual numerical solutions of Casson SA–hybrid nanofluid toward a stagnation point flow over stretching/shrinking cylinder, *Nanotechnology Reviews*, 13(1), 2024, 20230191.
[41] Awati, V.B., Goravar, A., Kumar, M., Bognar, G., Stability analysis of magnetohydrodynamic Casson fluid flow and heat transfer past an exponentially shrinking surface by spectral approach, *Case Studies in Thermal Engineering*, 60, 2024, 104810.
[42] Mahabaleshwar, U.S., Maranna, T., Mishra, M., Hatami, M., Sunden, B., Radiation effect on stagnation point flow of Casson nanofluid past a stretching plate/cylinder, *Scientific Reports*, 14(1), 2024, 1387.
[43] Mukhopadhyay, S., Vajravelu, K., Gorder, R.A.V., Casson Fluid Flow and Heat Transfer at an Exponentially Stretching Permeable Surface, *Journal of Applied Mechanics*, 80(5), 2013, 054502.
[44] Reddy, N.N., Rao, V.S., Reddy, B.R., Chemical reaction impact on MHD natural convection flow through porous medium past an exponentially stretching sheet in presence of heat source/sink and viscous dissipation, *Case Studies in Thermal Engineering*, 25, 2021, 100879.
[45] Turkyilmazoglu, M., The analytical solution of mixed convection heat transfer and fluid flow of a MHD viscoelastic fluid over a permeable stretching surface, *International Journal of Mechanical Sciences*, 77, 2013, 263-268.
[46] Ozturk, O., Explicit solutions of confluent hypergeometric equation with the help of differintegral theorems, *Dokuz Eylul University Faculty of Engineering Journal of Science and Engineering*, 18(3), 2016, 279-289.
[47] Campos, L.M.B.C., On some solutions of the extended confluent hypergeometric differential equation, *Journal of Computational and Applied Mathematics*, 137(1), 2001, 177-200.
[48] Qasim, M., Heat and mass transfer in a Jeffrey fluid over a stretching sheet with heat source/sink, *Alexandria Engineering Journal*, 52(4), 2013, 571-575.
[49] Kumar, A., Tripathi, R., Singh, R., Sheremet, M.A., Entropy generation on double diffusive MHD Casson nanofluid flow with convective heat transfer and activation energy, *Indian Journal of Physics*, 95, 2021, 1423-1436.
[50] Grubka, L.J., Bobba, K.M., Heat transfer characteristics of a continuous stretching surface with variable temperature, *Journal of Heat Transfer*, 107(1), 1985, 248-250.

ORCID iD

Sina Sadighi https://orcid.org/0000-0002-8920-2199
Goodarz Ahmadi https://orcid.org/0000-0001-5277-7960
Hossein Afshar https://orcid.org/0000-0002-6948-1581
Hossein Ahmadi Danesh Ashtiani https://orcid.org/0000-0001-6736-0500
Mohsen Jabbari https://orcid.org/0000-0003-0029-6668

How to cite this article: Sadighi S. et al., Parametric Study of Entropy Generation in Magnetohydrodynamic Casson Fluid Flow on a Porous Stretching Sheet under an Inclined Magnetic Field, *J. Appl. Comput. Mech.*, 11(3), 2025, 681-691. https://doi.org/10.22055/jacm.2024.47739.4778